Distributed electric current systems in solar active regions

Yuriy A. Fursyak **Valentina I. Abramenko** **Alexander S. Kutsenko**



Crimean Astrophysical Observatory of RAS, 298409, Nauchny, Crimea, Russia

e-mail: yuriy_fursyak@mail.ru

Abstract

Using data from the Helioseismic and Magnetic Imager on board the Solar Dynamics Observatory (HMI/SDO) on the magnetic field vector in the solar photosphere, we analyzed the structure of magnetic fields and vertical electric currents in six active regions (ARs) with different levels of flare activity. Decomposition of the transverse magnetic field vector into two components allowed us to reveal the existence of vortex structures of the azimuthal magnetic field component covering a large area around the main sunspots of an AR, which indicates to a presence of the distributed over large area electric current system. The low value of the vertical electric current imbalance over the entire AR (below 0.1%) suggests that the distributed electric current is closed within an AR. We calculated the distributed electric currents in all analyzed ARs and studied their temporal variations and the relationship with the flare productivity of an AR. It was found that low-flaring ARs exhibit small variations of the distributed electric current in the range of $\pm 20\times10^{12}$ A, whereas the highly flaring ARs exhibited significant smooth variations of the distributed current in the range of $(30\text{-}95)\times10^{12}$ A. Intervals of the enhanced flaring appear to be co-temporal with smooth enhancements of the distributed electric current.

Introduction

It is widely accepted that the energy released during solar flares and coronal mass ejections is stored in active regions (ARs) in the solar corona, in the form of the so-called "free" magnetic energy associated with the presence of electric currents (e.g. Abramenko, Gopasiuk, and Ogir', 1991; Melrose,1991; Wang et al., 1996; Schrijver et al., 2005; Aschwanden, 2013; Fleishman and Pevtsov, 2018; Toriumi and Wang, 2019, to mention a few).

We are engaged in the study of electric current systems in active regions with different levels of flare productivity. The features of our works are the application of the integral form of Ampere's law in the calculation of vertical electric currents, and a number of other non-standard solutions. So, in this study, we resume the method of detecting large-scale electric current structures in AR, which was first proposed in the work of Abramenko and Gopasyuk (1987), and then elaborated in the work of Abramenko, Gopasyuk and Ogir (1991). A distinctive feature of this method is the delineation of a relatively small contour in the vicinity of large spots in the AR according to certain rules. Magnetic elements of different polarities can be located inside such contour, which distinguishes our study from the number of works on the study of current structures in ARs (see, for example, Georgoulis, Titov, and Mikic, 2012; Kontogiannis et al., 2017), in which the calculation of electric currents is carried out over a large area covering magnetic elements of only one polarity.

The main objectives of this study are:

1) To show the presence of large-scale electric currents in active regions with non-zero flare productivity.
2) To establish the nature of the relationship between the time variations of the magnitude of a large-scale (here-distributed) electric current and the dynamics of the flash activity of AR.

Observational data

For our study we selected six ARs listed in Table 1. The guideline for selection was as follows. First, the set must represent both flare-quiet and flare-productive ARs. The top three ARs listed in Table 1 are low-flaring groups. The other three exhibited enhanced flaring activity. The ARs in Table 1 are ordered by increasing flare index, FI (fourth column in Table 1), which represents flare productivity of an AR (Abramenko, 2005) and equals 1 (100) for an AR that produced one C1.0 (X1.0) flare per day. Second, flaring ARs should represent the essential magnetic structures. Thus, NOAA AR 12158 is an anti-Hale group (with wrong leading polarity), AR 12371 is a bipolar, and AR 12192 is a multipolar group. The main data source used in this work was SDO/HMI vector magnetic field measurements provided by the Joint Science Operation Center (JSOC, http://jsoc.stanford.edu/). The spatial resolution of the instrument is 1 arcsec with a pixel size of 0.5×0.5 arcsec^2 and the temporal resolution for magnetic field vector data is 12 min. A special algorithm is used (Turmon et al., 2010) to automatically identify and crop AR patches from the full-disk magnetograms.

The patches of ARs are provided as Space-Weather Active Region Patches (SHARPs, Bobra et al., 2014). To minimize the influence of the projection effect we tracked ARs as long as they were located within ±35 degrees of the central meridian (corresponding to a four-day time interval, which are shown in the third column of Table 1). Flare activity of the ARs was evaluated using the 1-8 Å X-ray flux measurements acquired by the Geostationary Operational Environmental Satellite-15 (GOES-15, the data are available at https://satdat.ngdc.noaa.gov/sem/goes/data/full/). We also used images of the Sun acquired at the 1600 Å spectral line by the Atmospheric Imaging Assembly on board SDO (SDO/AIA: Lemen et al., 2012), to analyze the structure and dynamics of the associated flares.

Table 1 Parameters of the ARs under study.

NOAA number	Lat. deg.	Obs. interval	FI	$\langle\Phi\rangle$ 10^{22} Mx	$\langle I_{tot}\rangle$ 10^{15} A	$\langle I_{net}\rangle$ 10^{12} A	$\langle I_{distr}\rangle$ 10^{12} A	$\langle\rho_{j_z}\rangle$ %	$\langle\rho_{B_z}\rangle$ %
12674	N14	2017 Sep. 03–06	0.76	2.47	3.74	−1.27	5.98	−0.034	−9.270
12494	S12	2016 Feb. 05–07	1.02	0.73	1.13	0.37	8.23	0.033	−14.757
12381	N14	2015 Jul. 07–10	5.43	1.38	2.37	−1.78	2.91	−0.075	0.039
12158	N15	2014 Sep. 09–12	13.30	1.45	2.48	0.54	−12.53	0.022	3.970
12371	N13	2015 Jun. 20–23	20.13	2.97	3.36	3.26	23.60	0.097	2.125
12192	S14	2014 Oct. 22–25	123.44	9.53	10.51	6.52	58.14	−0.062	−2.074

Methods used

We used the integral form of Ampère's law to compute the electric current density at each pixel of a magnetogram:

$$j_z = \frac{1}{\mu_0 s}\oint_L \boldsymbol{B_t} d\boldsymbol{r},$$

where the integration is performed over a small closed contour L enclosing an areas where the vertical electric current density is to be calculated. Our previous study (Fursyak, 2018) showed that a contour size of 5×5 pixels is the best compromise between the noise level and loss of information due to smoothing by the integration. Typical distributions of local vertical electric currents in AR are shown in Fig. 1.

For each magnetogram acquired during the analyzed period we calculated the unsigned total vertical current, I_{tot}, as a sum of absolute values of the current density multiplied by the pixel area. The averaged over time I_{tot} are presented in the sixth column of Table 1. We can see that the magnitudes are nearly similar (except for the strongest AR 12192), suggesting that the flare-quiet and flare-productive ARs do not significantly differ.

We also calculated the imbalance of the local currents and the magnetic flux (their time averaged values are listed in the last two columns of Table 1). We used the commonly accepted formula for the imbalance (Abramenko, Wang and Yurchishin, 1996):

$$\rho_{j_z} = \frac{\sum_{S+}|j_z(i,j)| - \sum_{S-}|j_z(i,j)|}{\sum_{S+}|j_z(i,j)| + \sum_{S-}|j_z(i,j)|} \times 100\%,$$

where jz(i, j) is the electric current density at pixel (i, j), S+ (S−) denotes a set of pixels with jz(i, j) > 0 (jz(i, j) < 0).

The current imbalance for six studied ARs is very low (it does not exceed 0.1%), whereas the flux imbalance can be quite strong (see last two columns of Table 1). This implies that the vertical electric currents of all scales are closing within an AR, whereas a significant fraction of the magnetic flux of an AR may close elsewhere outside the AR.

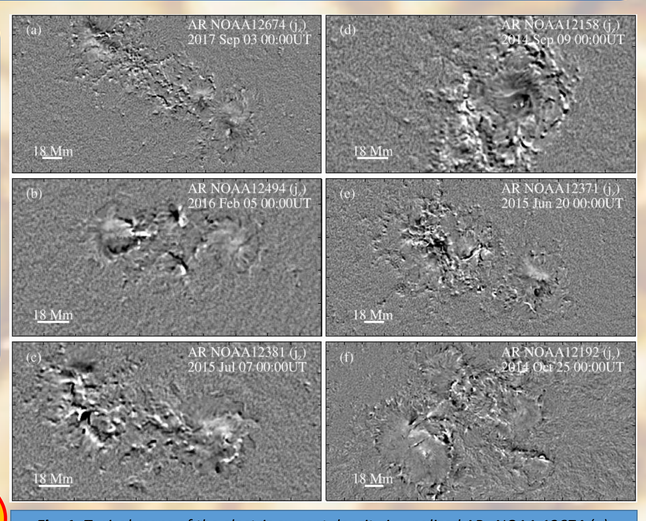

Fig. 1. *Typical maps of the electric current density in analized ARs NOAA 12674 (a), 12494 (b), 12381 (c), 12158 (d), 12371 (e), and 12192 (f). The maps are scaled from −0.02 A m^{-2} (black) to 0.02 A m^{-2} (white).*

Structured local electric currents and elongated current ribbons of both signs could be seen in the current distribution maps in Fig. 1. If the surface-distributed current does exist, it is not readily visible in these maps. To reveal it we used a method introduced and tested in Abramenko and Gopasyuk (1987). A distributed vertical electric current can manifest itself as a regular deviation from potentiality, i.e. as an organized vortex-like azimuthal magnetic field. Therefore, one may detect distributed electric currents by analyzing the deviation of the observed magnetic field lines from the corresponding potential configuration.

Thus, to detect a distributed electric current, we performed the following steps (see also Fig. 2):

Step I. For each vector magnetogram, we calculated a potential magnetic field based on the observed B_z component using the IDL CFF1N code (Sakurai, 1982).

Step II. In each pixel of the magnetogram, we compare the vector of the potential transverse magnetic field and the vector of the observed transverse magnetic field of AR.

Step III. The vector of the observed transverse magnetic field is decomposed into two components - along (the potential component of the transverse magnetic field of AR), and across the vector of the potential field (the non-potential component of the observed field). The latter component is due to the presence of electric currents in the AR.

Step IV. If we further isolate only the non-potential component, then in the vicinity of large spots of AR, we can detect a regular vortex structure due to the presence of a large-scale electric current distributed over a large area of AR, which we call a distributed electric current. To calculate the value of the distributed electric current, it is necessary to outline the contour C around the spot so that inside this contour the direction of rotation of the vector of the non-potential component has one predominant direction - clockwise or counterclockwise, and then sum up the values of the electric current in each pixel of the selected contour:

$$I_{distr} = \int_S j_z ds.$$

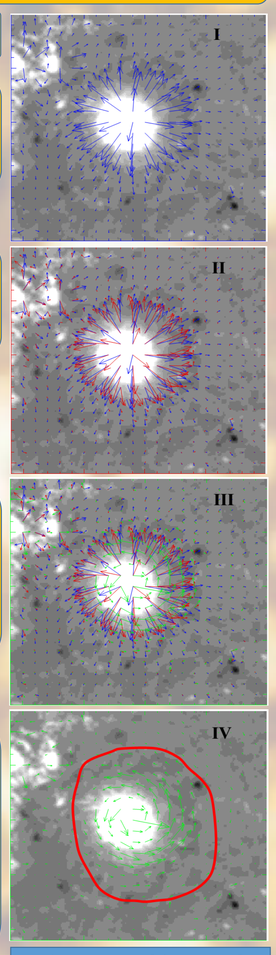

Fig. 2. *Stages of detection of distributed electric current*

The sign of I_{distr} is positive when the resulting current is directed toward the observer and negative in the opposite case (in this case, prevails counterclockwise rotation of the vector of the non-potential component of the transverse magnetic field). The time-averaged I_{distr} for each AR are presented in the eighth column of Table 1. Data in this table show that for all ARs the net current over a magnetogram, I_{net}, is weaker than the net current inside a contour, I_{distr}. This implies that the outlining of a specific contour to detect the global structure with prevailing current really makes sense.

The contour was defined on the first magnetogram, the shape of the contour was kept the same during the observational interval and the location of the contour was fixed relative to the center of gravity of the sunspot. Note that the summation of electric currents is performed for all pixels inside the contour C, regardless of the polarity of the magnetic elements. This distinguishes our study from the works of other researchers in this field which consider the summation of currents separately by positive and negative magnetic polarities.

Since the imbalance of vertical electric currents in the AR is very low, we believe that the distributed electric current detected by us spreads to the upper layers of the solar atmosphere in one part of the AR, and closes through the chromosphere and the corona on the remaining part of the AR. Therefore, the distributed electric current must be associated with solar flares.

Results

We found large-scale electric current systems in all six studied ARs. Two distributed current systems were found in the NOAA 12192 region, one of which was associated with a large sunspot of negative polarity in the tail part of the AR. We analyzed this particular current system, since it was associated with the strongest solar flares in the AR. It is interesting that this system of electric current is also recreated by model calculations (see Fig. 3 and study Jiang et al., 2016).

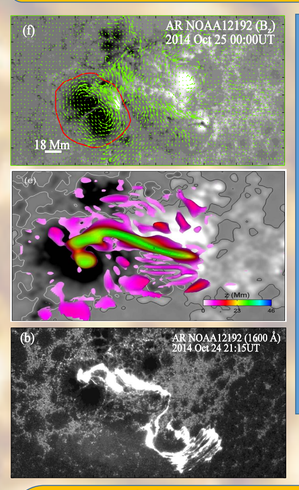

Fig. 3. *Top - line-of-sight magnetogram and the vector of the non-potential component of the transverse magnetic field (green arrows) for AR NOAA 12192. Red thick curves show the chosen contours C used to calculate the magnitude of distributed electric current. In center - results of MHD modeling. Top view of a volume with a current density exceeding the average value by more than 20 times. The color indicates the height from the bottom boundary. This picture is taken from the article Jiang et al., 2016. Bottom - UV 1600 Å AIA/SDO image of AR NOAA 12192 during flare event X3.1 on 24 October 2016, showing flare ribbon that coincide spatially with the direction of the distributed current in the AR.*

Since, as we believe, the distributed electric current goes up high into the chromosphere and the corona, we set ourselves the task of investigating time variations in the magnitude of the distributed electric current and compared them in each case with the dynamics of the flare productivity of AR. The time variations of the distributed electric current in studied ARs, along with other AR parameters are shown in Fig. 4.

We found that the magnitude of the distributed current was changing with time. Thus, flare-quiet ARs (see Fig. 4, red curves) show a rather low magnitude of I_{distr} (in a range of $\pm 20\times10^{12}$ A), and the sign of I_{distr} can change as well. This behavior may be explained by intrusion of new strong small scale local electric currents into the vortex area driven by sudden appearance/disappearance of magnetic features. ARs with high flare productivity show a much higher level of I_{distr} (up to 90×10^{12} A), so that the possible disturbances by small-scale current features do not affect the sign of I_{distr} and time variations of the I_{distr} magnitude are very gradual.

We also found that periods of enhanced flaring (M- and X-class flares) are nearly co-temporal with the high level of distributed electric current.

Conclusions

1. In all cases the imbalance of local vertical currents over the entire magnetogram was found to be very low (from 0.02 to 0.1%) and it remained persistently low during the entire studied time interval (4 days). At the same time, imbalance of the vertical magnetic field was much higher (up to 14%). This finding implies that, first, vertical electric currents of all scales are closed inside the AR and, second, the magnetic field and electric currents do not always follow each other, so that the photospheric magnetic field either is not a force-free field, or a part of the magnetic flux is potential and leaves an AR.
2. In the active region with non-zero flash activity, there are electric current systems of various scales. In addition to local vertical electric currents, we found large-scale electric currents distributed over a large area and covering the entire AR or a significant part of it, which we called distributed electric currents.
3. Taking into account the low imbalance of electric currents in the AR, it can be assumed that the distributed current spread out into the upper layers of the solar atmosphere in one part of the AR and closes through the chromosphere and corona on the remaining part of the AR.
4. The magnitude of the distributed electric current and its dynamics are different for ARs with different levels of flare productivity. Low-flaring ARs exhibit small variations of the distributed currents in the range of $\pm 20\times10^{12}$ A, whereas the highly flaring ARs exhibited significant slow variations of the distributed currents in the range of $(30\text{-}90)\times10^{12}$ A. Intervals of the enhanced flaring appear to be co-temporal with smooth enhancements of the distributed electric current.

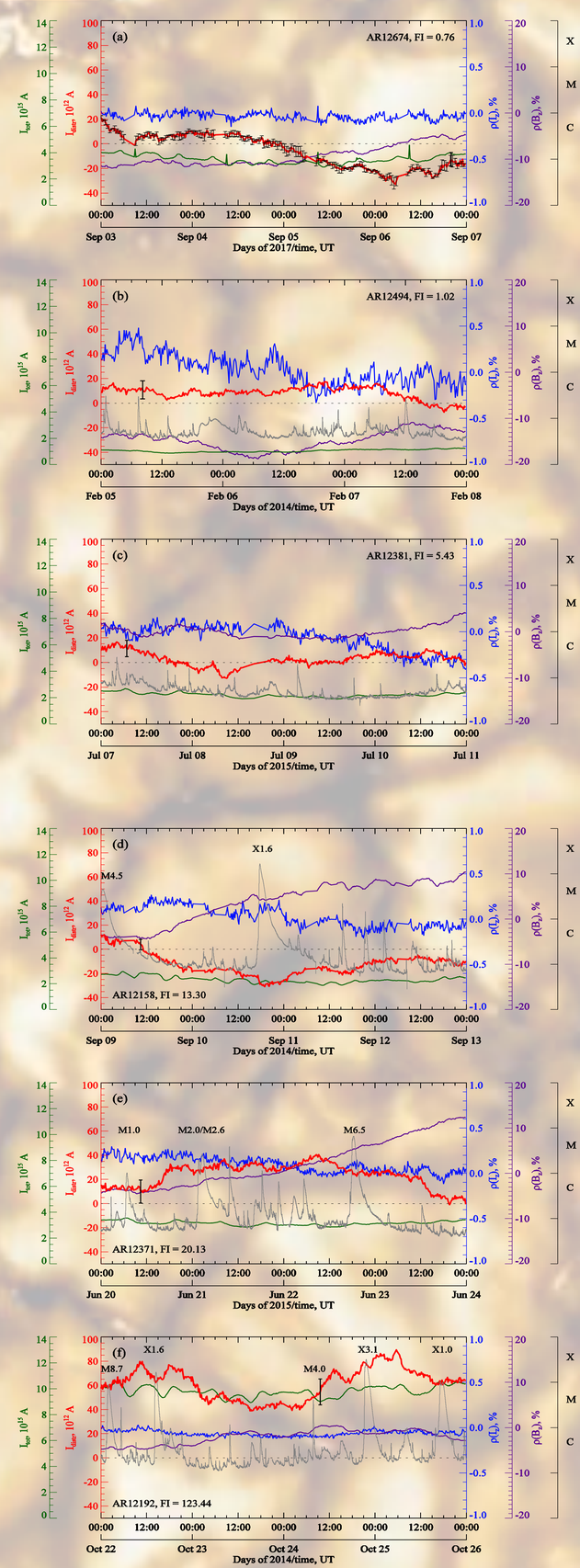

Fig. 3. *Time variations of the distributed electric current magnitude (red), total electric current (green), electric current imbalance (blue), and magnetic flux imbalance (violet) for a sample of flare-quiet ARs. GOES-15 X-ray flux is shown in gray. On the top panel the GOES flux is omitted because of a strong domination of the neighbor NOAA AR 12673.Error bars in calculations of I_{distr} for each third magnetogram are shown for AR 12674, the highest error is marked as a solid bar. For the rest of ARs, only the highest error bar is shown.*

This study was supported by Russian Science Foundation (RSF), project No. 18-12-00131.

Literature

Abramenko, V.I.: 2005, Astrophys. J. **629**, 1141.
Abramenko V.I., Gopasiuk S.I., Ogir', M.B.: 1991, Solar Phys. **134**, 287.
Abramenko V.I., Gopasyuk S.I.: 1987 Bull. Crimean Astrophys. Obs. **76**, 163.
Abramenko V.I., Wang T., Yurchishin V.B.: 1996, Solar Phys. **168**, 75.
Aschwanden M.J.: 2013, Solar Phys. **287**, 369.
Bobra M.G., Sun, X., Hoeksema J.T., Turmon M., Liu Y., et al.: 2014, Solar Phys. **289**, 3549.
Fleishman G.D., Pevtsov A.A. Electric Currents in Geospace and Beyond **43**, Am. Geophys. Union, Washington, 2018.
Fursyak Y.A.: 2018, Geomagn. Aeron. **58**, 1129.
Georgoulis M.K., Titov V.S., Mikic Z.: 2012, Astrophys. J. **761**, 61.
Kontogiannis I., Georgoulis M.K., Park S.-H., Guerra J.A.: 2017, Solar Phys. **292**, 159.
Lemen J.R., Title A.M., Akin D.J., Boerner P.F., Chou C., et al.: 2012, Solar Phys. **275**, 17.
Melrose D.B.: 1991, Astrophys. J. **381**, 306.
Jiang C., Wu S.T., Yurchyshyn V., Wang H., Feng X., Hu Q.: 2016, Astrophys. J. **828**, 62.
Sakurai T.: 1982, Solar Phys. **76**, 301.
Schrijver C.J., De Rosa M.L., Title A.M., Metcalf T.R.: 2005, Astrophys. J. **628**, 501.
Toriumi S., Wang H.: 2019, Living Rev. Solar Phys. **16**, 3.
Turmon M., Jones H.P., Malanushenko O.V., Pap J.M.: 2010, Solar Phys. **262**, 277.
Wang J., Shi Z., Wang H., Lue Y.: 1996, Astrophys. J. **456**, 861.